

Incorporating energy metabolism into a growth model of multicellular tumor spheroids

Raja Venkatasubramanian, Michael A. Henson, Neil S. Forbes*

Department of Chemical Engineering, University of Massachusetts, 159 Goessmann Laboratory, 686 North Pleasant Street, Amherst, MA 01003-9303, USA

Received 30 August 2005; received in revised form 13 March 2006; accepted 17 March 2006

Available online 2 May 2006

Abstract

Diffusion limitations in tumors create regions that are deficient in essential nutrients and contain a large number of quiescent and dying cells. Chemotherapeutic compounds are not effective against quiescent cells and therefore have reduced efficacy against tumors with extensive quiescence. We have formulated a mathematical model that predicts the extent and location of quiescence in multicellular spheroids. Multicellular spheroids are *in vitro* models of *in vivo* tumor growth that have proven to be useful experimental systems for studying radiation therapy, drug penetration, and novel chemotherapeutic strategies. Our model incorporates a realistic description of primary energy metabolism within reaction–diffusion equations to predict local glucose, oxygen, and lactate concentrations and an overall spheroid growth rate. The model development is based on the assumption that local cellular growth and death rates are determined by local ATP production generated by intracellular energy metabolism. Dynamic simulation and parametric sensitivity studies are used to evaluate model behavior, including the spatial distribution of proliferating, quiescent, and dead cells for different cellular characteristics. Using this model we have determined the critical cell survival parameters that have the greatest impact on overall spheroid physiology, and we have found that oxygen transport has a greater effect than glucose transport on the distribution of quiescent cells. By predicting the extent of quiescence based on individual cellular characteristic alone this model has the potential to predict therapeutic efficiency and can be used to design effective chemotherapeutic strategies.

© 2006 Elsevier Ltd. All rights reserved.

Keywords: Multicellular tumor spheroid; Energy metabolism; Tumor growth modeling; Quiescence; Hypoxia; Diffusion

1. Introduction

Chemotherapeutic compounds that show promise in monolayer culture studies often prove substantially less effective in tumors due to pronounced diffusion limitations in key nutrients such as glucose and oxygen which produce nutrient deficient regions that eventually become necrotic in tumors *in vivo*. *In vitro* multicellular spheroids mimic the heterogeneous microenvironments present in *in vivo* three-dimensional (3-D) tissues which are not present in monolayer cultures (Kunz-Schughart, 1999; Sutherland, 1988). The development of mathematical models that predict the effect of nutrient diffusion on spheroid microenvironment and growth has received considerable attention. When combined with a suitable experimental

effort, such predictive models can be used to guide the design of improved chemotherapeutic strategies.

Idealized tumor spheroids possess desirable mathematical properties such as radial symmetry, which have facilitated the derivation of tumor growth models. A common modeling objective is to predict the formation of the three cell classes commonly observed in tumors *in vivo*: (1) proliferating cells located near the perimeter of the spheroid where favorable nutritional conditions lead to rapid cell growth and division; (2) quiescent cells located further inside the spheroid where the local nutritional environment is not sufficient for significant proliferation but is adequate to ensure cell survival; and (3) necrotic cells located near the interior of the spheroid which have died due to prolonged exposure to poor nutritional conditions. Several mathematical models that describe the diffusion of nutrients and growth/inhibitory factors between the surrounding environment and the spheroid have been

*Corresponding author. Tel.: +1 413 577 0132; fax: +1 413 545 1647.

E-mail address: forbes@ecs.umass.edu (N.S. Forbes).

developed (Araujo and McElwain, 2004). Typically, these models are based on the assumption of a single growth limiting species. Growth models that combine diffusion equations with reaction-convection equations for the expanding spheroid also have been presented (Adam and Maggelakis, 1989, 1990; Chaplain and Britton, 1993; Greenspan, 1976; Pettet et al., 2001; Sherratt and Chaplain, 2001; Ward and King, 1997). A recent study investigated the role of acidity on the growth and invasion of cells in vascular and avascular tumors (Smallbone et al., 2005). Tumor growth models have also been used to study the effects of drug diffusion and drug-induced cell death on spheroid growth (Bertuzzi et al., 2003; Jackson and Byrne, 2000; Ward and King, 2003). While they provide useful insights into tumor growth dynamics, these models are based on overly simplified descriptions of cellular metabolism that limit their effectiveness as predictive models.

The tumor spheroid model presented in this paper is based on the hypothesis that diffusion limitations create spatial nutrient gradients that alter local energy metabolism, which in turn affects overall spheroid physiology. Cancer cells are known to consume considerably more glucose than normal cells under identical conditions (Newsholme and Leech, 1983). While tumor cells oxidize a portion of the glucose they uptake, a large fraction is converted to lactate. Analysis of tumor interstitial fluid suggests that the tricarboxylic acid (TCA) cycle is saturable, which could explain the high rate of lactate production (Helmlinger et al., 2002). Two independent clinical trials have shown that high lactate (Brizel et al., 2001; Walenta et al., 1997, 2000) and low oxygen concentrations (Brizel et al., 1996) in *in vivo* tumors are each correlated with increased likelihood of metastases, tumor recurrence, and reduced patient survival. The presence of hypoxia is known to reduce the effectiveness of radiation therapy, as this treatment strategy is dependent on presence of oxygen radicals (Vaupel et al., 2001). We believe that the incorporation of primary energy metabolism within a reaction-diffusion model of tumor growth has the potential to explain observed nutrient concentration profiles and tumor physiology such as hypoxia and central necrosis. Although we recognize that growth factors are critical for promoting mammalian cell growth, they are not included in our model under the assumption that their diffusion and utilization are not limiting and that cell death is primarily due to limited nutrient supply.

Other researchers have developed spheroid models in which the growth and death of multiple cell types are affected by a single limiting nutrient (Pettet et al., 2001; Sherratt and Chaplain, 2001; Ward and King, 1997). To our knowledge, only one previous modeling study attempts to connect cellular metabolism and tumor physiology (Casciari et al., 1992). While a reasonably detailed description of energy metabolism was included, the spheroid model was based on an average cellular growth rate obtained by integrating the local growth rate across

the spheroid radius. By contrast, our model allows spatial variations in the growth rate consistent with the prevailing nutritional microenvironment. We utilize an extended version of a previously developed model (Ward and King, 1997) to describe spheroid morphology and growth. The cell population is partitioned into intact live (proliferating and quiescent) and dead (necrotic) cells with fixed volumes. Volume generation within the spheroid is assumed to create a radial velocity gradient that results in spheroid expansion. The novelty of our model is that the diffusion of multiple nutrients (glucose, oxygen and lactate) is coupled to a metabolic model that accounts for glycolysis, the TCA cycle and lactate production/consumption. Consistent with our basic hypothesis concerning energy metabolism, the cellular growth and death rates are parameterized in terms of the ATP generation rate obtained from the metabolic model. A simple method to partition the live cell population into proliferating and quiescent cells is developed to allow more detailed analysis of spheroid morphology.

2. Multicellular spheroid model

2.1. Live cell density

The cell population is assumed to be comprised of intact living and dead cells with fixed volumes. Let $\ell(r, t)$ and $d(r, t)$ represent the live and dead cell number densities, respectively, where the assumption of radial symmetry allows only a single spatial coordinate r to be used. Then the following conservation equations hold (Ward and King, 1997):

$$\frac{\partial \ell}{\partial t} + \nabla \cdot (v\ell) = (\mu_g - \mu_d)\ell \quad \ell(r, 0) = 1 \quad (1)$$

$$\frac{\partial d}{\partial t} + \nabla \cdot (vd) = \mu_d d \quad d(r, 0) = 0 \quad (2)$$

where μ_g and μ_d are the rates of cell growth and death, respectively, v is the bulk convective velocity of the cell mass, and the initial condition represents a homogeneous population of live cells. The growth and death rates are dependent on the cellular energy state, which is determined by the local nutrient environment. The cells are assumed to be tightly packed such that void space can be neglected:

$$V_L \ell + V_D d = 1 \quad (3)$$

where V_L and $V_D < V_L$ represent the average volumes of a living cell and a dead cell, respectively. This relation allows the conservation Eq. (2) for dead cells to be eliminated from the model.

2.2. Convective velocity

Spheroid expansion is assumed to be driven by the relative rates of cell growth and death. Cell growth produces an instantaneous volume increase, while cell

death results in an instantaneous loss of volume. Local volume changes produce a radial velocity gradient in the cell mass described by the following equation that follows from directly Eqs. (1)–(3) (Ward and King, 1997):

$$\nabla \cdot v = \mu_g \ell V_L - \mu_d \ell (V_L - V_D) \quad v(0, t) = 0 \quad (4)$$

where the boundary condition enforces zero velocity at the center of the spheroid. The rate of spheroid growth is determined by evaluating the velocity at the spheroid boundary:

$$\frac{dR}{dt} = v(R, t) \quad R(0) = R_{Cell} \quad (5)$$

where R_{Cell} is the initial spheroid radius, which corresponds to that of a single live cell:

$$R_{Cell} = \left(\frac{3V_L}{4\pi} \right)^{1/3} \quad (6)$$

2.3. Nutrient transport

Our metabolic model is based on the assumption that tumor cells can consume three nutrients: glucose, oxygen, and lactate. The following nutrient transport equations are obtained under the standard assumption that transport processes are much faster than spheroid growth dynamics:

$$D_i \nabla^2 c_i = Q_i(c, t) \ell, \quad c_i(R, t) = c_{i,Bulk}, \quad i = Gluc, \quad (7)$$

$$\nabla c_i(0, t) = 0, \quad Lac, Ox$$

where c_i is the local nutrient concentration in the spheroid interior, $c_{i,Bulk}$ is the bulk nutrient concentration outside the spheroid, D_i is the nutrient diffusion coefficient, Q_i is the nutrient uptake rate that depends on the vector \underline{c} containing all the nutrient concentrations. We have neglected mass transfer limitations such that the nutrient concentrations at the spheroid perimeter are equal to their associated bulk concentrations.

2.4. Metabolic description

The model of primary energy metabolism incorporated into the overall multicellular spheroid model contains the basic enzymic reactions of glycolysis and the TCA cycle involving three key metabolites: glucose, oxygen, and lactate (Fig. 1). This simple model of intracellular metabolism relates the cellular uptake of nutrients to the amount of available energy (ATP) in a cell, and ultimately relates cellular growth and death rates to extracellular metabolite concentrations.

The uptake rate of each extracellular metabolites is based on the availability of the nutrient in the extracellular environment and the stoichiometric limitations of intracellular metabolism. Three transmembrane transport equations represent the maximum uptake rates based on extracellular nutrient concentrations. The transmembrane uptake rates are the upper limits of the metabolic uptake

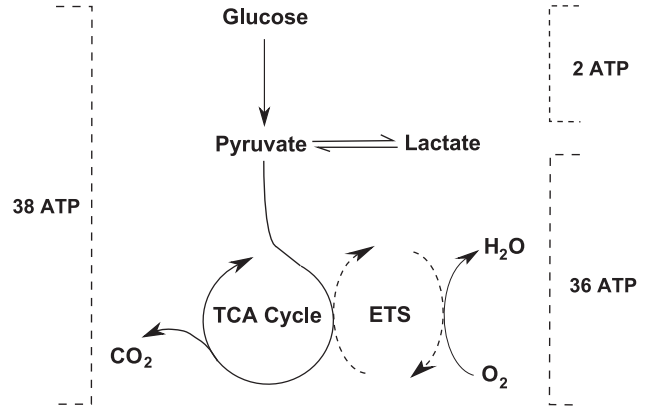


Fig. 1. Model of primary energy metabolism that was incorporated into the multicellular spheroid model. The three metabolites included in the model are glucose, oxygen and lactate. Consumed glucose is converted into pyruvate, which is either converted into CO₂ in the TCA cycle or excreted as lactate. In the presence of oxygen, lactate can be consumed and converted into CO₂ in the TCA cycle. The amount of ATP generated by each pathway can be determined based on the assumption that all reductive equivalents are converted into ATP by the electron transport system (ETS), which consumes oxygen and produces water. The ATP production from the conversion of glucose to pyruvate, the conversion of lactate to pyruvate, and the oxidation of pyruvate are 8, 3, and 15 ATP molecules, respectively. The net ATP production, as indicated, for the complete oxidation of glucose is 38 ATP molecules, 8 + (2 × 15); for the conversion of glucose into two lactate molecules is 2 ATP molecules, 8 – (2 × 3); and the oxidation of two lactate molecules is 36 ATP molecules, (2 × 3) + (2 × 15).

rates and are described using the following Michaelis–Menten equations:

$$Q_{Gluc,transmembrane} = \frac{Q_{Gluc,max} c_{Gluc}}{K_{m,Gluc} + c_{Gluc}} \quad (8)$$

$$Q_{Ox,transmembrane} = \frac{Q_{Ox,max} c_{Ox}}{K_{m,Ox} + c_{Ox}} \quad (9)$$

$$Q_{Lac,transmembrane} = \frac{Q_{Lac,max} c_{Lac}}{K_{m,Lac} + c_{Lac}} \quad (10)$$

These simple hyperbolic functions state that when metabolite is not present, it cannot be consumed by cells, and when the concentration of metabolite is high, the uptake rates are saturated at their maximum values ($Q_{Gluc,max}$, $Q_{Ox,max}$, $Q_{Lac,max}$).

To determine the actual metabolic uptake rates an additional set of constraints are introduced to account for the stoichiometry of intracellular metabolism. These constraints are based upon a simple set of assumptions:

1. Cells will consume glucose when it is available.
2. All reductive equivalents (NADH and FADH) are converted into ATP by the electron transport system (ETS).
3. Lactate can be consumed as a carbon source when the concentration of glucose is low and the concentration of oxygen is high.

4. The P/O ratios for NADH and FADH₂ are 3 and 2, respectively (Newsholme and Leech, 1983).

Based on assumption one, glucose uptake is limited only by its transport across the cell membrane:

$$Q_{Gluc} = Q_{Gluc, transmembrane} \quad (11)$$

In contrast to glucose, oxygen uptake can be limited either by its own transmembrane transport or by transmembrane transport of glucose and lactate. When the extracellular concentration of oxygen is low, the transmembrane uptake of oxygen ($Q_{Ox, transmembrane}$) will be limiting. However, when the concentrations of glucose and lactate are low, the stoichiometry of intracellular metabolism will limit the rate of oxygen uptake. Based on assumption 2, all reductive equivalents (NADH and FADH₂) generated by glycolysis and the TCA cycle are converted into ATP by the ETS, which consumes oxygen and produces water. The complete oxidation of one molecule of glucose consumes six molecules of O₂ and the oxidation of one molecule of lactate in the TCA cycle consumes three molecules of O₂:

$$Q_{Ox} = \min(Q_{Ox, transmembrane}, 6Q_{Gluc} + 3Q_{Lac, transmembrane}) \quad (12)$$

The rate of lactate consumption and/or production is dependent on the rates of glucose and oxygen uptake, and is determined by the stoichiometry of the intracellular reactions. One molecule of glucose can produce two molecules of lactate and the oxidation of one molecule of lactate requires three molecules of oxygen

$$Q_{Lac} = -2Q_{Gluc} + Q_{Ox}/3 \quad (13)$$

This stoichiometric balance describes both the production ($Q_{Lac} < 0$) and consumption ($Q_{Lac} > 0$) of lactate. If the uptake of glucose is stoichiometrically greater than the uptake of oxygen, then the excess glucose will be converted into lactate. Conversely, if the uptake of oxygen is stoichiometrically greater than the uptake of glucose, then lactate will be consumed and oxidized as a carbon source (assumption 3). Note that the uptake of oxygen can only be stoichiometrically greater than the uptake of glucose if lactate is present in the environment ($Q_{Lac, transmembrane} > 0$). This limitation is implicit in Eq. (12).

The ATP produced by glycolysis, the TCA cycle, and the consumption of lactate is used to estimate overall ATP generation. Based on assumptions 2 and 4, the conversion of 1 glucose molecule into 2 pyruvate molecules would produce 8 molecules of ATP as glycolysis produces 2 ATP molecules and 2 NADH molecules, which are equivalent to 6 ATP molecules (assumption 4). Similarly, the conversion of 1 lactate molecule into 1 pyruvate molecule would produce 1 NADH molecule, which is equivalent to 3 ATP molecules. The complete oxidation of 1 pyruvate molecule would consume 3 oxygen molecules and would produce 4 NADH molecules, 1 FADH₂ molecule, and 1 GTP molecule, which are equivalent to 15 ATP molecules.

Thus, each oxygen molecule consumed in complete oxidation of pyruvate in the TCA cycle is considered to produce an equivalent of 5 ATP molecules. When combined, these relations indicate that the complete oxidation of 1 glucose molecule would produce 38 equivalent ATP molecules, the conversion of 1 glucose molecule into 2 lactate molecules would produce 2 ATP molecules, and the oxidation of 2 lactate molecules would produce 36 equivalent ATP molecules (Fig. 1). This analysis is based on the assumption that one molecule of pyruvate requires three molecules of oxygen to be oxidized in the TCA cycle (assumption 4). Therefore, the net ATP production rate can be related to the consumption rates of glucose and oxygen by the simple expression:

$$Q_{atp} = 8Q_{Gluc} + 3Q_{Lac} + 5Q_{Ox} = 2Q_{Gluc} + 6Q_{Ox} \quad (14)$$

The first equality follows from the proceeding discussion, and the second equality is obtained by solving Eq. (13) for Q_{Lac} and substituting the result into Eq. (14).

2.5. Cellular growth and death rates

A basic premise of our model is that the growth and death rates are determined by cellular energetics as reflected by the local ATP generation rate. A hyperbolic-type equation is used to represent the growth rate dependence:

$$\mu_g = \frac{\mu_{g, max} Q_{atp}}{K_{g, atp} + Q_{atp}} \quad (15)$$

where the parameters $\mu_{g, max}$ and $K_{g, atp}$ are the maximum cellular growth rate and cell growth saturation constant, respectively. The functional form for the death rate is

$$\mu_d = \mu_{d, max} \left(1 - \frac{\sigma Q_{atp}}{K_{d, atp} + Q_{atp}} \right) \quad (16)$$

where σ is the basal survival rate, which is complimentary to the basal death rate, $1 - \sigma$. This parameter was included in the model to account for cell death that is independent of metabolism and cellular energetics (Ward and King, 1997); e.g. apoptosis due to nuclear damage.

2.6. Proliferating and quiescent cell populations

The live cell population consists of both rapidly proliferating cells and quiescent cells, which can be viewed as either very slowly growing or cell cycle arrested in the G0 phase. Further partitioning of the live cell population into proliferating and quiescent cells is useful since many chemotherapeutic strategies effectively target only rapidly proliferating cells (Hietanen et al., 1995; Siu et al., 1999). While models that explicitly account for proliferating and quiescent cells have been proposed (Byrne and Chaplain, 1995; Pettet et al., 2001; Sherratt and Chaplain, 2001), we have lumped these cells into a single population due to the experimental difficulty of determining the transitions rates

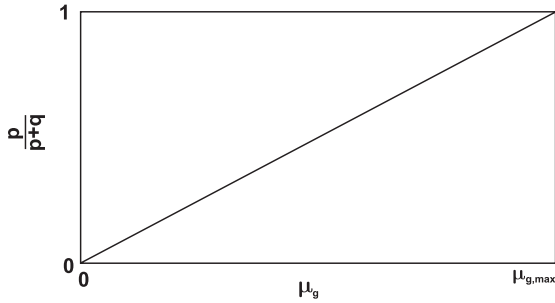


Fig. 2. The population of live cells was partitioned into proliferating and quiescent cell populations assuming a linear dependence on the cellular growth rate.

between the proliferating and quiescent cell populations. On the other hand, our model does not allow different metabolic activities to be ascribed to the proliferating and quiescent populations. This increased level of granularity, which is necessary to describe the reduced nutrient uptakes and growth rates of quiescent cells, will be included in our future modeling studies.

As an alternative, we have developed a partitioning method based on the assumption that all living cells are rapidly proliferating when nutritional conditions allow growth at the maximum rate $\mu_{g,max}$. By contrast, all living cells are assumed to be quiescent at zero growth rates. Linear interpolation is used to estimate the fraction of proliferating cells at intermediate growth rates (Fig. 2), thereby producing the following relations between the densities of live cells $\ell(r,t)$, proliferating cells $p(r,t)$ and quiescent cells $q(r,t)$:

$$p(r,t) = \frac{\mu_g(r,t)}{\mu_{g,max}} \ell(r,t) \quad (17)$$

$$q(r,t) = \left(1 - \frac{\mu_g(r,t)}{\mu_{g,max}}\right) \ell(r,t) \quad (18)$$

This method will tend to overestimate the quiescent cell density because it is based on the assumption that proliferating cells are always growing at the maximum rate $\mu_{g,max}$. However, this method is consistent at the limits ($\mu_g = \mu_{g,max}$ and $\mu_g = 0$) and should therefore provide useful information about the morphology of tumor spheroids under different nutritional conditions.

2.7. Non-dimensionalization

The following dimensionless variables are introduced:

$$\begin{aligned} \tilde{t} &= \frac{t}{(1/\mu_{g,max})}, & \tilde{v} &= \frac{v}{(R(t)\mu_{g,max})}, \\ \tilde{\ell} &= \frac{\ell}{(1/V_L)}, & \tilde{d} &= \frac{d}{(1/V_D)}, & \tilde{r} &= \frac{r}{R(t)}, \\ R(0) &= \left(\frac{3V_L}{4\pi}\right)^{1/3}, \end{aligned}$$

$$\begin{aligned} \tilde{c}_{Gluc} &= \frac{c_{Gluc}}{c_{Gluc,Bulk}}, & \tilde{c}_{Lac} &= \frac{c_{Lac}}{c_{Gluc,Bulk}}, & \tilde{c}_{Ox} &= \frac{c_{Ox}}{c_{Ox,Bulk}}, \\ \delta &= \frac{V_D}{V_L}, & \tilde{\mu}_g &= \frac{\mu_g}{\mu_{g,max}}, & \Gamma &= \frac{\mu_{d,max}}{\mu_{g,max}}, \\ \tilde{Q}_i(\tilde{c}) &= \frac{Q_i(c)}{Q_{imax}}, & \tilde{K}_{m,i} &= \frac{K_{m,i}}{c_{i,Bulk}} \end{aligned} \quad (19)$$

The inverse of the maximum growth rate is used as the characteristic time. All time-dependent parameters, including the local growth rate, μ_g , and the local death rate, μ_d , are normalized by the maximum growth rate, $\mu_{g,max}$. Non-dimensionalization leads to the following set of equations, which need to be solved simultaneously:

$$\frac{1}{\tilde{r}^2} \frac{\partial}{\partial \tilde{r}} \left(\frac{\partial \tilde{c}_i}{\partial \tilde{r}} \right) = Da_i(t) \tilde{Q}_i(\tilde{c}) \tilde{\ell} \quad (20)$$

$$\begin{aligned} \left(\frac{\partial \tilde{c}_i}{\partial \tilde{r}} \right)_{\tilde{r}=0, \tilde{t}} &= 0, & \tilde{c}_{Glucose}(\tilde{r}=1, \tilde{t}) &= 1, & \tilde{c}_{Oxygen}(\tilde{r}=1, \tilde{t}) &= 1, \\ \tilde{c}_{Lactate}(\tilde{r}=1, \tilde{t}) &= 0, \end{aligned}$$

$$\begin{aligned} \frac{\partial \tilde{\ell}}{\partial \tilde{t}} + \tilde{v} \frac{\partial \tilde{\ell}}{\partial \tilde{r}} &= (\alpha(\tilde{c}) - \beta(\tilde{c}) \tilde{\ell}) \tilde{\ell}, \\ \left(\frac{\partial \tilde{\ell}}{\partial \tilde{r}} \right)_{\tilde{r}=0, \tilde{t}} &= 0 \quad \tilde{\ell}(\tilde{r}, \tilde{t}=0) = 1 \end{aligned} \quad (21)$$

$$\begin{aligned} \frac{1}{\tilde{r}^2} \frac{\partial(\tilde{r}^2 \tilde{v})}{\partial \tilde{r}} &= \beta(\tilde{c}) \tilde{\ell}, \\ \tilde{v}(\tilde{r}=0, \tilde{t}) &= 0 \end{aligned} \quad (22)$$

where the dimensionless parameters Da_i , α and β are defined as follows:

$$\begin{aligned} Da_i(t) &= \frac{R(t)^2 Q_i \mu_{g,max}}{D_i V_L c_{i,Bulk}} \quad i = \text{Glucose, Lactate or Oxygen} \\ \tilde{c} &= [\tilde{c}_{Glucose} \quad \tilde{c}_{Oxygen} \quad \tilde{c}_{Lactate}]^T \\ \alpha(\tilde{c}) &= (\tilde{\mu}_g - \tilde{\mu}_d) & \beta(\tilde{c}) &= (\tilde{\mu}_g - (1 - \delta) \tilde{\mu}_d) \end{aligned} \quad (23)$$

2.8. Numerical solution

The spheroid growth model consists of a coupled set of nonlinear partial differential, ordinary differential, and algebraic equations with a moving outer boundary. We used an iterative calculation procedure and spatial discretization with a moving grid to numerically solve the model equations. At each time point t_i , the spheroid radius $R(t_i)$ was used to map the radial domain to unit length and orthogonal collocation on finite elements (Finlayson, 1980) was used to compute the grid points. We used 100 finite elements and 4 internal collocation points to produce the simulation results presented in this paper. A velocity of $v(R(t_i))$ was assigned to the outermost grid point located on the spheroid perimeter such that this point had the local velocity of the moving boundary (Crank, 1984). A unique velocity was assigned to each interior grid point to ensure that these points remained stationary with respect to the

outermost point. Therefore, the following modified form of Eq. (21) was written for each grid point j :

$$\left(\frac{d\ell}{dt}\right)_j = v_j \frac{\partial v}{\partial r} + \left(\frac{d\ell}{dt}\right)_r, \quad v_j = \frac{r_j v(R(t))}{R(t)}, \quad j = \text{grid node} \quad (24)$$

The discretization procedure generated a coupled set of nonlinear ordinary differential and algebraic equations with time as the only independent variable. The discretized equations were solved simultaneously over a small time interval $\Delta t = 0.005$ using the differential-algebraic equation (DAE) solver DASPK 2.0 (Brown et al., 1994, 1995) to generate results for the next time point $t_{i+1} = t_i + \Delta t$. DASPK options were used to exploit the considerable sparsity of the Jacobian matrix and to calculate a consistent set of initial conditions for the DAE system. An updated spheroid radius $R(t_{i+1})$ was determined by integrating the non-dimensionlized version of Eq. (5) with an explicit Euler scheme using a constant velocity $v(R(t_{i+1}))$ over the Δt time interval. The iterative procedure was repeated until the final simulation time was reached. A related spheroid growth model was solved using a similar iterative procedure in which radial discretization was performed using finite difference approximation and an adaptive mesh that concentrates points near the spheroid perimeter (Ward and King, 1997). Our numerical solution method produced stable and converged solutions without resorting to adaptive meshing as long as a sufficient number of mesh points were used.

3. Results and discussion

3.1. Base case results

The first set of simulation results were generated using the nominal parameter values listed in Table 1. To the extent possible, parameter values were obtained from appropriate literature sources. The parameters associated with lactate uptake and the ATP dependence of cell growth and death were adjusted to obtain reasonable model behavior. More specifically, the maximum lactate uptake rate and the lactate uptake saturation constant ($Q_{Lac,max}$ and $K_{Lac,max}$) were chosen to prevent lactate uptake from constraining cellular metabolism. The cell growth and death saturation constants ($K_{g,atp}$ and $K_{d,atp}$) were set close to zero such that cells survived when energy was available and appreciable cell death only occurred when energy dropped below a very low threshold. We present parametric sensitivity analysis of the multicellular spheroid model in the next section. The results of this analysis will be used to guide our future experimental studies aimed at estimating the key model parameters.

Spheroid expansion was characterized by a slow exponential growth phase followed by a transition to a linear growth phase after approximately 10 days (Fig. 3). The spheroid growth rate in the linear phase was approximately 150 $\mu\text{m}/\text{day}$, which is very close to values obtained experimentally (Casciari, 1989; Landry et al., 1982). The four dots in Fig. 3 correspond to spheroid radii of one living cell (initial condition), 50 μm (4.5 days),

Table 1
Model parameter values and their literature sources

Symbol	Description	Value	Source
<i>Experimentally derived parameters</i>			
D_{Gluc}	Glucose diffusion coefficient	$1.05 \times 10^{-6}(\text{cm}^2/\text{s})$	Casciari et al. (1988)
$Q_{Gluc,max}$	Maximum glucose uptake rate	$1.33 \times 10^{-16}(\text{mol}/(\text{cell sec}))$	Casciari et al. (1992)
$K_{m,Gluc}$	Glucose uptake saturation constant	$4.0 \times 10^{-2}(\text{mM})$	Casciari et al. (1992)
D_{Ox}	Oxygen diffusion coefficient	$1.82 \times 10^{-3}(\text{cm}^2/\text{s})$	Mueller-Klieser and Sutherland (1984)
$Q_{Ox,max}$	Maximum oxygen uptake rate	$7.16 \times 10^{-17}(\text{mol}/(\text{cell sec}))$	Casciari et al. (1992)
$K_{m,Ox}$	Oxygen uptake saturation constant	$4.64 \times 10^{-3}(\text{mM})$	Casciari et al. (1992)
D_{Lac}	Lactate diffusion coefficient	$1.78 \times 10^{-6}(\text{cm}^2/\text{s})$	Casciari et al. (1992)
$\mu_{g,max}$	Maximum cell growth rate	$4.95 \times 10^{-2}(\text{h}^{-1})$	Ward and King (1997)
V_L	Living cell volume	$4.975 \times 10^{-9}(\text{cm}^3)$	Casciari et al. (1992)
<i>Literature-derived dimensionless parameters</i>			
Γ	Ratio of maximum cell death rate to maximum cell growth rate	1	Ward and King (1997)
Σ	Basal survival rate	0.9	Ward and King (1997)
Δ	Ratio of dead cell volume to living cell volume	0.5	Ward and King (1997)
<i>Other parameters</i>			
$Q_{Lac,max}$	Maximum lactate uptake rate	$1 \times 10^{-14}(\text{mol}/(\text{cell sec}))$	
$K_{m,Lac}$	Lactate uptake saturation constant	$5.5 \times 10^{-4}(\text{mM})$	
$K_{g,atp}$	Cell growth saturation constant	$3.75 \times 10^{-19}(\text{mol}/\text{cells})$	
$K_{d,atp}$	Cell death saturation constant	$3.75 \times 10^{-19}(\text{mol}/\text{cells})$	

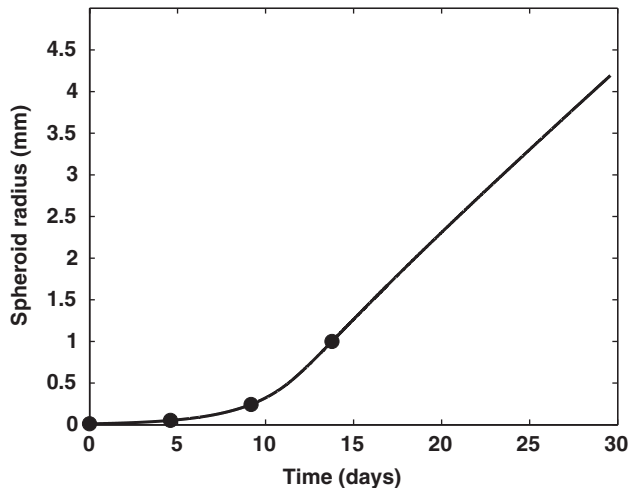


Fig. 3. Growth of the outer spheroid radius, $R(t)$, for the nominal model parameter values. The four indicated time points correspond to spheroid radii of one living cell (the initial condition), $50\ \mu\text{m}$ (4.5 days), $250\ \mu\text{m}$ (9.2 days) and $1\ \text{mm}$ (13.7 days).

$250\ \mu\text{m}$ (9.2 days) and $1\ \text{mm}$ (13.7 days). Although not included in the present model because degradation of cellular material has been neglected (Ward and King, 1999), experimentally observed growth saturation (Freyer, 1988; Freyer and Sutherland, 1986) precludes spheroid expansion beyond a radius of about $1\ \text{mm}$.

Asymptotically the spheroid model produced a traveling wave solution, as demonstrated by the transient live cell density and bulk velocity profiles (Fig. 4). The live cell density quickly decreased from an initial condition of all live cells to a value of approximately 0.9 that was maintained near the spheroid perimeter during subsequent growth (Fig. 4a). Dead cells are present in the well-supplied periphery because of the inclusion of a non-zero basal death rate, $1-\sigma$, which was incorporated in the model to account for causes of cell death other than nutritional limitations. The velocity at the spheroid perimeter plateaus at a constant value, which is consistent with the existence of a linear growth phase that has been observed experimentally (Landry et al., 1982). The fully developed velocity profile was characterized by a region of positive velocity at the periphery due to the presence of predominantly proliferating cells and a region of negative velocity located further inside the spheroid due to volume loss caused by cell death (Fig. 4b).

Fig. 5 shows glucose and oxygen concentration profiles for spheroid radii of one living cell (initial condition), $50\ \mu\text{m}$ (4.5 days), $250\ \mu\text{m}$ (9.2 days) and $1\ \text{mm}$ (13.7 days) corresponding to the points in Fig. 3. Analogous results for lactate concentration and ATP production profiles are shown in Fig. 6. As expected, nutrient diffusion limitations were not observed during the initial stages of spheroid growth. After approximately 10 days, cells located near the center of the spheroid began to encounter low nutrient concentrations (Fig. 5), which caused reduced ATP

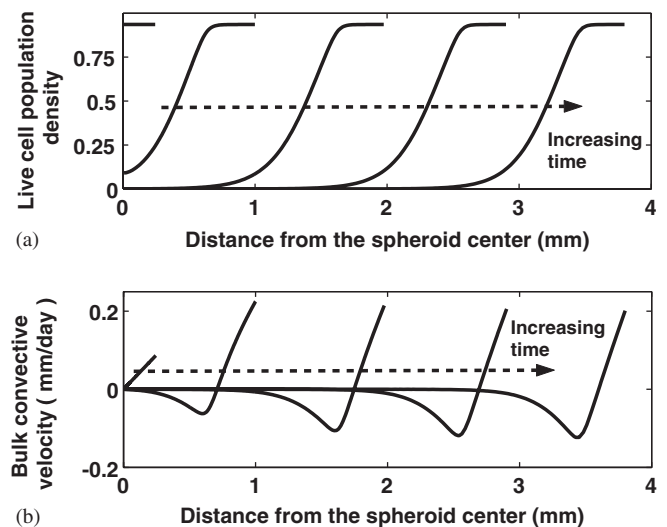


Fig. 4. Evolution of (a) the live cell number density and (b) the radial velocity as a function of spheroid radius at various stages of spheroid growth.

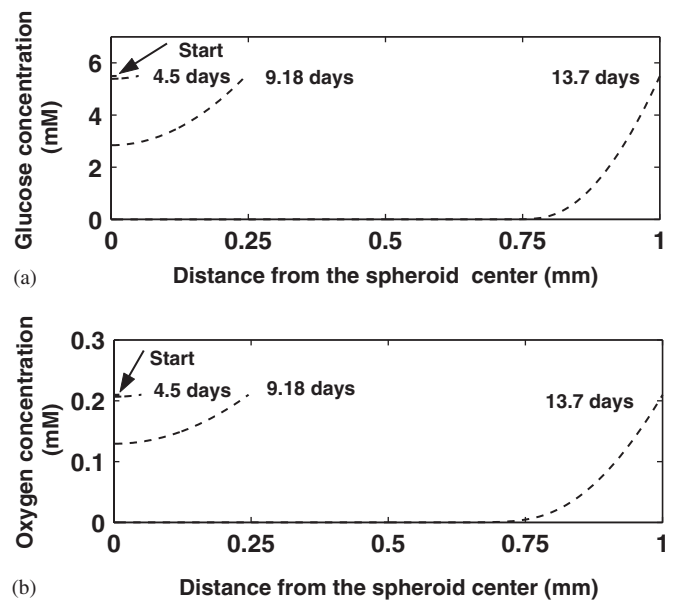


Fig. 5. Evolution of (a) the glucose concentration profile and (b) the oxygen concentration profile at four stages of spheroid growth: one living cell (Start), $50\ \mu\text{m}$ radius (4.5 days), $250\ \mu\text{m}$ radius (9.2 days) and $1\ \text{mm}$ radius (13.7 days).

production (Fig. 6b). The model predicted that oxygen was completely consumed within $300\ \mu\text{m}$ of the spheroid perimeter, which is consistent with experimental observations (Acker et al., 1987). Severe nutrient limitations were observed throughout most of the spheroid after approximately 14 days of growth. A pronounced decrease in ATP production was caused by low interior nutrient concentrations, and the live cell density decreased substantially as a result (Fig. 4a). ATP production was approximately constant near the spheroid perimeter, implying that both glucose and oxygen were taken up at their maximum

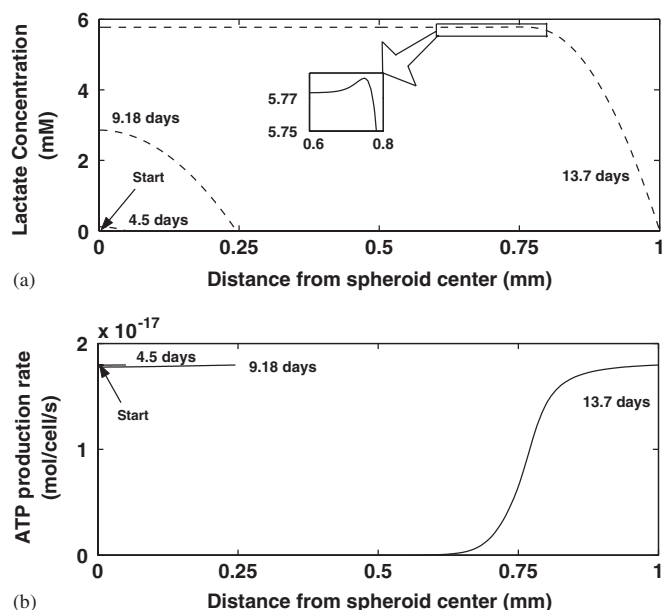


Fig. 6. Evolution of (a) the lactate concentration profile and (b) the ATP production profile at four stages of spheroid growth: one living cell (Start), 50 μm radius (4.5 days), 250 μm radius (9.2 days) and 1 mm radius (13.7 days). The inset in the lactate concentration plot shows a region of lactate re-absorption between $r = 0.65$ and 0.8 mm for a 1 mm radius spheroid.

possible rates. The observed lactate concentration profiles (Fig. 6a) resulted from lactate production due to aerobic glycolysis. Tumor cells have been known to metabolize nutrients via aerobic glycolysis despite the low energy efficiency (Newsholme and Leech, 1983). Lactate production occurs in the region where glucose availability exceeds oxygen availability in a stoichiometric sense. A small amount of lactate was consumed in large spheroids (inset in Fig. 6a), generating a very small peak in the lactate concentration profile. This result showed that glucose was completely consumed and then lactate was used as a carbon source until available oxygen was completely depleted.

The live cell population was partitioned into proliferating and quiescent cells for a simulated spheroid of 1 mm radius (Fig. 7). The model produced the three distinct regions (proliferating, quiescent, and necrotic) experimentally observed in large spheroids. The outer region was dominated by proliferating cells due to the locally favorable nutritional conditions. As nutrient diffusion limitations became pronounced, the proliferating cell density dropped sharply to yield a smaller middle region dominated by quiescent cells. The low nutrient concentrations predicted near the spheroid center produced a large inner necrotic region dominated by dead cells.

3.2. Parametric studies

Parametric studies were performed to determine sensitivities with respect to a set of metrics that characterize the physiology of a spheroid. The results from the sensitivity

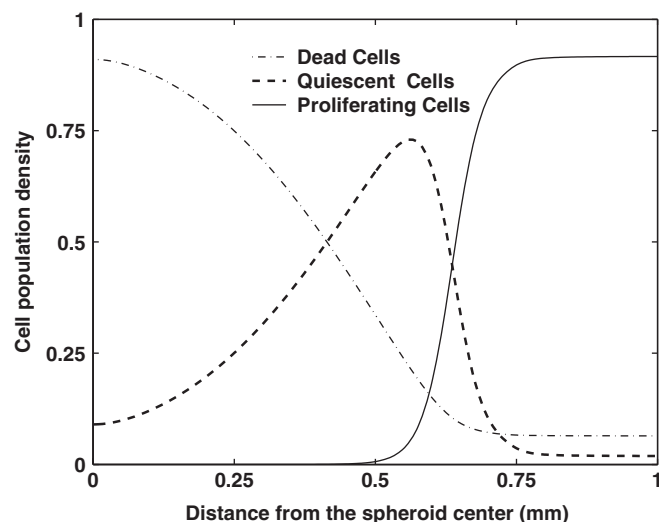


Fig. 7. Distribution of cell types in a spheroid of 1 mm radius. Proliferating cells are located at the periphery ($r > 0.5$), dead cells are primarily located in the interior ($r < 0.6$), and quiescent cells are located between these two populations.

analysis will be useful in directing laboratory and clinical experimentation. Many of the model parameters are expected to vary between cancer cell lines and between individual cancer patients. The parameters that have the largest predicted effect on spheroid physiology will be the focus of future investigations to determine how significantly they vary.

Two types of metrics were defined to characterize spheroid physiology as a function of spheroid radius: (1) metrics that describe cellular populations and (2) metrics that describe nutrient conditions. Cell population metrics are important outputs of the model because they are indicative of chemotherapeutic efficacy. Most chemotherapeutics specifically act on proliferating cells and are ineffective on quiescent cells (Hietanen et al., 1995; Siu et al., 1999). The location and number of quiescent cells in a spheroid gives an indication of the number of cells that will survive a dose of chemotherapy.

All metrics were determined for a fixed spheroid radius of 1 mm to eliminate the size dependence. The locations of proliferating and quiescent cells were defined relative to the outer edge of the spheroid. The penetration depth of proliferating and quiescent cells was defined as the point where the proliferating and quiescent cell number density equaled 10% of its maximum value. The total numbers of proliferating, quiescent, and dead cells were calculated from the cell number densities and the volume of live (V_L) and dead (V_D) cells. These metrics were chosen because they are routinely measured in our laboratory, which will make validation of the model predictions relatively straightforward.

The composition profiles of glucose and oxygen were characterized by the depth at which the concentrations equaled 1% of their values in the bulk media. These penetration depths indicate where diffusion becomes limiting

and nutrient concentrations are not predominately controlled by cellular uptake rates. The ATP production penetration depth was defined as the distance from the periphery where the ATP production rate equals $K_{g,atp}$. Beyond this depth, limited ATP generation decreases the rate of growth and increases the rate of death.

Both local and large perturbation sensitivity analyses were performed to investigate model behavior. Local sensitivity analysis was performed by increasing each parameter individually by 1% of its base case value (Table 1) to approximate the effect of an infinitesimally small parameter change. The sensitivity, $S(j,k)$, was defined as the ratio of the relative change in metric M_k to the relative change in parameter P_j following a parameter change from P_j^0 to P_j^*

$$S(j,k) = \frac{P_j^0}{M_k^0} \frac{M_k^* - M_k^0}{P_j^* - P_j^0} \quad (25)$$

Here M_k^0 and M_k^* are the values of the k th metric before and after perturbation, respectively. Normalized values were used to ensure that sensitivity values could be compared across all parameters and metrics. In this paper, sensitivity values greater than 10% are considered significant.

Large perturbation analysis was performed to identify qualitative trends in model behavior and to predict the growth behavior of spheroids composed of cell types with different physiologies. The model parameters describe individual cell characteristics, while the metrics are associated with spheroid (or cell population) characteristics. Parameters that are predicted to cause the most significant changes in the metrics will have the greatest effect on spheroid behavior. Most parameters were perturbed from 50% to 200% of their base case values to encompass a wide range of potential values. For the non-dimensional parameters (Γ , σ , and δ), smaller perturbations were performed. For example, the basal death rate, σ , was varied from a lower bound of 0.5 to an upper bound of 1.0.

3.2.1. Parameters for uptake and diffusion of metabolites

Local sensitivity analysis indicated that diffusion of oxygen had a greater impact on the cell population metrics

than the diffusion of glucose. The parameter that directly control the oxygen concentration profile, the maximum oxygen uptake rate, $Q_{Ox,max}$, had significant impact on all of the metrics except for the glucose penetration depth (Table 2). Alternately, the parameter that directly control the glucose concentration profile, the maximum glucose uptake rate, $Q_{Gluc,max}$, did not significantly impact any of the cell population metrics, except the glucose penetration depth (Table 2). The strong dependence of the cell population metrics on oxygen diffusivity and uptake parameters indicates that oxygen is essential for the growth and survival of cells in spheroids and that hypoxia is the primary condition that induces growth arrest.

Oxygen penetration had greater control over cell survival and death because at the nominal parameter values, glucose was consumed first and oxygen was able to penetrate deeper into the spheroid. Large perturbation analysis indicated that as the maximum glucose uptake rate, $Q_{Gluc,max}$, was increased, the ATP penetration depth paralleled the oxygen penetration depth and oxygen availability was limiting (right-hand side of Fig. 8). However, when $Q_{Gluc,max}$ was decreased beneath 75% of its baseline level, the ATP penetration depth paralleled the glucose penetration depth, indicating that glucose was limiting (left-hand side of Fig. 8). Thus, oxygen uptake was limiting at the nominal value of $Q_{Gluc,max}$, explaining why the population metrics, which are dependent on ATP production, were more sensitive to oxygen uptake around the baseline values.

Large perturbation analysis further showed that doubling the maximum oxygen uptake rate, $Q_{Ox,max}$, shifted the ATP production rate to a regime where glucose became limiting (Fig. 9a). As $Q_{Ox,max}$ was increased, the ATP penetration depth paralleled the oxygen penetration depth until the threshold was reached and the dependence of the ATP penetration became parallel to the glucose penetration depth. This change in ATP penetration subsequently impacted the proliferating and quiescent cell penetration depths (Fig. 9b). $Q_{Ox,max}$ affected the penetration depths in the regime where its value was low and oxygen availability was limiting, but it had a minimal effect in the regime where its value was high and glucose availability was

Table 2

Local sensitivity analysis of maximum glucose uptake rate ($Q_{Gluc,max}$), maximum oxygen uptake rate ($Q_{Ox,max}$), maximum lactate uptake rate ($Q_{Lac,max}$), normalized maximum death rate (Γ), basal survival rate (σ), the saturation parameters for growth ($K_{g,atp}$), and death ($K_{d,atp}$), live cell volume (V_L) and the dead to live cell volume ratio (Δ)

Metric	$Q_{Ox,max}$	$Q_{Gluc,max}$	$Q_{Lac,max}$	Γ	σ	$K_{g,atp}$	$K_{d,atp}$	V_L	Δ
Glucose penetration depth	-0.004	-0.514	0	0.037	-0.274	0.001	0.006	0.531	0.033
Oxygen penetration depth	-0.520	-0.001	0	0.046	-0.282	0.001	0.008	0.605	0.041
Proliferating region penetration	-0.520	0	0	0.037	-0.270	-0.064	0.007	0.546	0.033
Total number of proliferating cells	-0.266	0.028	0	-0.083	0.381	-0.069	-0.027	-0.661	-0.031
Quiescent penetration depth	-0.614	-0.001	0.003	-0.883	0.747	-0.050	-0.052	0.793	-0.158
Total number of quiescent cells	0.457	0.053	0.002	-0.463	1.300	0.213	-0.058	-1.548	-0.367
Total number of dead cells	0.665	0.065	-0.004	0.961	-3.384	0.053	0.195	-1.817	0.599

Sensitivities were calculated by perturbing each parameter +1% and calculating the relative change in the metric as defined by Eq. (25).

Values greater than 0.1(10%) were considered significant and are in bold.

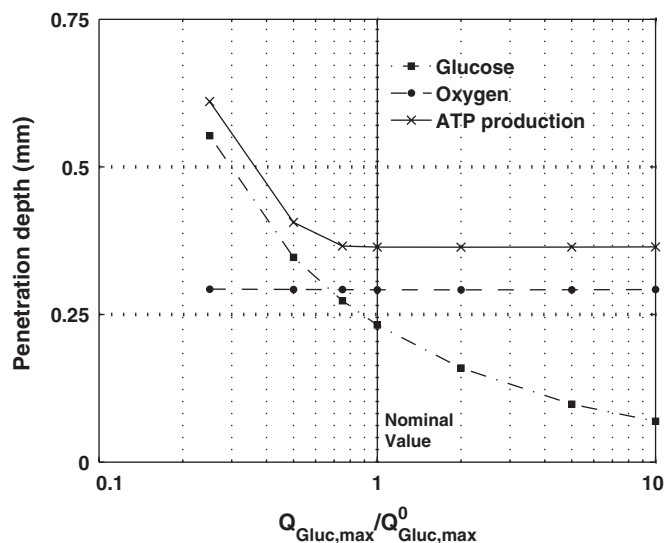
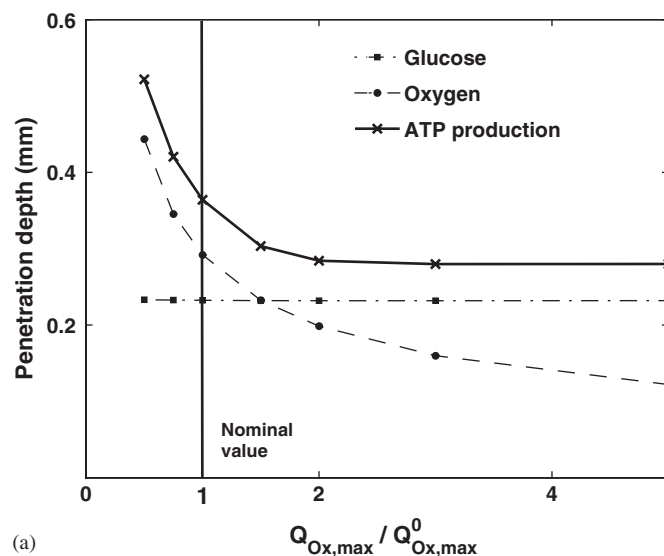


Fig. 8. Changes in the glucose, oxygen and ATP production penetration depths following large perturbations in the maximum glucose uptake rate. The maximum glucose uptake rate ($Q_{Gluc,max}$) is shown relative to the nominal maximum glucose uptake rate ($Q_{Gluc,max}^0$). At high values the ATP production penetration depth was parallel to the oxygen penetration depth. When glucose availability became limiting ($Q_{Gluc,max}/Q_{Gluc,max}^0 < 0.7$), the ATP production penetration depth paralleled the glucose penetration depth.

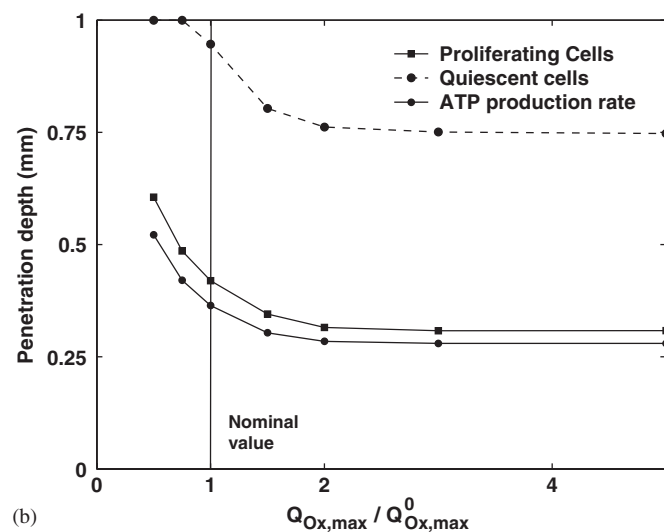
limiting. The quiescent cell penetration depth saturated at 1 mm for low values of $Q_{Ox,max}$ because the analysis was based on a 1 mm radius spheroid. Although the width of the quiescent region did not change considerably, the total number of quiescent cells increased with increasing $Q_{Ox,max}$ (Table 2) because the quiescent region moved towards the outside of the spheroid, thereby increasing its volume.

Local sensitivity analysis showed that the maximum lactate uptake rate, Q_{Lac} , did not have significant impact on any of the metrics (Table 2). This minimal effect was anticipated because the parameters for lactate were chosen such that lactate uptake would not limit cellular metabolism. The low sensitivity values support these parameter choices.

Together these results give an indication of how cell survival is dependent on glucose and oxygen penetration in spheroids. At the baseline parameter values the population metrics were more strongly dependent on oxygen availability. However, when the maximum glucose uptake rate was decreased 25% or the maximum oxygen uptake rate was increased 100% the population metrics switched their dependence to glucose availability. It has been known for a long time that cancerous cells have glucose uptake rates as high as 10-fold greater than normal cells (Warburg, 1929). Tissues composed of non-transformed cells could therefore have a maximum glucose uptake rate 10% of the nominal value for a transformed cell line (Table 1). This suggests that glucose transport limitations play a more critical role in non-transformed tissues and oxygen transport limitations are more critical to transformed tissues. This result also suggests that cell death present in hypoxic tumors is



(a)



(b)

Fig. 9. Effect of large perturbations in the maximum oxygen uptake rate on the cell population metrics. The maximum oxygen uptake rate ($Q_{Ox,max}$) is shown relative to the nominal maximum oxygen uptake rate ($Q_{Ox,max}^0$): (a) Effect on the glucose, oxygen and ATP production penetration depths. At high values of $Q_{Ox,max}$, the ATP production penetration depth was parallel to the glucose penetration depth. When oxygen availability became limiting ($Q_{Ox,max}/Q_{Ox,max}^0 < 2.0$), the ATP production penetration depth paralleled the oxygen penetration depth. (b) Effect on the cell population penetration metrics. For all values of $Q_{Ox,max}$, the proliferating cell penetration depth was parallel to the ATP production penetration depth. The quiescent cell penetration depth increased with decreasing values of $Q_{Ox,max}$ until it reached the center of the spheroid ($Q_{Ox,max}/Q_{Ox,max}^0 < 0.75$).

caused by the high rate of glucose consumption present in transformed cells. Our inclusion of lactate production into the model allowed this dependence on oxygen availability to be observed.

3.2.2. Parameters for cell growth and death

As expected, the normalized maximum death rate, Γ , significantly affected the penetration of quiescent cells and the number of quiescent and dead cells (Table 2). However,

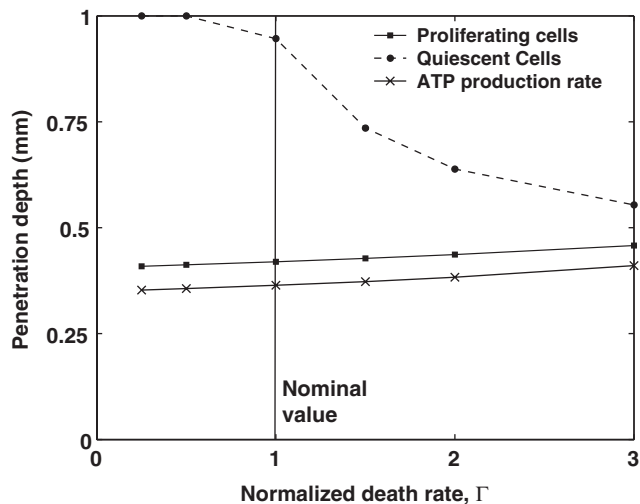


Fig. 10. Effect of large perturbations in the maximum normalized death rate, Γ , on the cell population metrics. The proliferating cell penetration depth consistently decreased with decreasing values of Γ and paralleled the ATP production penetration depth. The quiescent cell penetration depth increased considerably with decreasing values of Γ and saturated once quiescent cells reached the center of the spheroid ($\Gamma < 0.5$).

Γ did not significantly impact the penetration of nutrients or proliferating cells. Large perturbation analysis was performed to explain why Γ had a greater effect on the penetration depth of quiescent cells than proliferating cells (Fig. 10). Within the interior of the spheroid ($r < 0.6$ mm), the ATP production rate was almost zero (Fig. 6b). At this depth, quiescent cells were present (Fig. 7), but they were dying at close to the maximum possible rate, Γ . Therefore, in this regime Γ was the model parameter that had the greatest effect on cell survival. On the other hand, in the viable region of the spheroid ($r > 0.6$ mm) the proliferating cell penetration depth was directly proportional to the local growth rate (Fig. 2), which was tightly coupled to the ATP production rate (Eq. (15)). Changes in Γ had a minimal effect on the penetration depth of ATP production and therefore did not affect the proliferating cell penetration depth (Fig. 10).

The reduction in cell density in the outer regions of the spheroid as a result of increasing Γ did not significantly impact the penetration of nutrients. We anticipated that there would be a greater effect of the death rate on nutrient uptake. Perturbations in Γ did not affect nutrient and ATP production penetration depths because both quiescent and proliferating cells are assumed to consume nutrients at equal rates. The small changes in the proliferating cell and ATP production penetration depths in Fig. 10 were caused by the reduced number of cells in the outer region of the spheroid with increasing Γ .

The basal survival rate, σ , had a significant effect on all of the metrics (Table 2). The basal death rate is related to the basal survival rate as $1 - \sigma$. Both small and large perturbations of σ had opposite effects on the penetration depths of proliferating and quiescent cells (Table 2).

Decreasing σ from its nominal value of 0.9 caused the proliferating region to move deeper into the spheroid and the quiescent region to become shallower (not shown). Decreasing σ also caused the penetration depths of glucose, oxygen and ATP production to increase. An overall increase in cell death produced a reduced number of living cells in the periphery of the spheroid, which in turn decreased nutrient uptake per volume and enabled nutrients to penetrate deeper.

The seemingly contradictory effects of σ perturbations on the proliferating and quiescent penetration depths can be explained by the competition between two mechanisms: (1) the availability of nutrients in the local microenvironment; and (2) the effect of increased cell death throughout the spheroid. The model was formulated such that the boundary between proliferating and quiescent cells is determined by the growth rate, which is entirely dependent on the ATP production rate (Eq. (15)) and is independent of cell viability. Therefore the penetration depth of proliferating cells was controlled by nutrient availability (mechanism 1) and was independent of cell death (mechanism 2). Therefore, nutrients and proliferating cells were able to penetrate deeper into the spheroid as σ decreased. By contrast, the penetration depth of quiescent cells was controlled by both mechanisms. While increased nutrient availability enhanced growth, the decreased basal survival rate reduced the number of quiescent cells compared to dead cells. At the nominal parameter values, the effect of increased cell death outweighed the effect of increased nutrient availability causing the quiescent cell penetration depth to move outwards.

These predictions indicate that the basal survival rate, σ , is an important parameter that should be accurately determined by experiments. The high sensitivity of the metrics to this parameter indicates that the number and location of quiescent cells in a tumor will be highly dependent on the rate of cell death due to mechanisms not associated with cellular energy metabolism. The basal survival rate can be measured in both cell culture and animal models using standard staining and histological techniques. We expect that this parameter could vary considerably between tumor cells of different lineage. The less of an effect σ has for a specific cell type, the more accurately energy metabolism alone will predict the cell population distribution in 3-D tissue.

The saturation parameters for the cell growth and death rates, $K_{g,atp}$ and $K_{d,atp}$, did not significantly affect most of the metrics (Table 2). This set of results was unexpected because these two parameters represent the limiting ATP production rates where cellular growth and death processes become significant. Large perturbation analysis showed that the effect of these saturation parameters could be divided into two regimes (not shown). The lower regime in which the metrics were insensitive to the saturation parameters is reflected by the local sensitivities in Table 2. By contrast, when each saturation constant was increased

Table 3

Local sensitivity analysis of the saturation parameters for growth ($K_{g,atp}$) and death ($K_{d,atp}$) when their nominal values were increased by a factor of 20

Metric	$K_{g,atp}$	$K_{d,atp}$
Glucose penetration depth	0.2190	0.1292
Oxygen penetration depth	0.2734	0.1724
Proliferating region penetration	−0.1754	−0.0016
Total number of proliferating cells	−0.2522	−0.4975
Quiescent penetration depth	−0.0733	−0.1485
Total number of quiescent cells	−0.5316	0.1445
Total number of dead cells	0.4070	0.2851

Sensitivities were calculated by perturbing each parameter +1% and calculating the relative change in the metric as defined by Eq. (25). Values greater than 0.1(10%) were considered significant and are in bold.

by a factor of 20 the cell population metrics become more sensitive to these two parameters (Table 3). The nominal values of $K_{g,atp}$ and $K_{d,atp}$ were chosen to be in the lower regime and close to zero to be consistent with our assumption that cells do not stop growing and start dying until they are almost completely depleted of energy. In the lower regime the metrics were not affected by perturbations because of the steepness of the ATP production rate profile. In the upper regime the ATP profile is flatter and small changes in $K_{g,atp}$ and $K_{d,atp}$ produce larger changes in the growth and death rates, and therefore in the cell population metrics.

The assumption that the values of $K_{g,atp}$ and $K_{d,atp}$ are close to zero can be tested experimentally. The rate of ATP production can be estimated from glucose and oxygen uptake measurements through stoichiometric analysis. Approximate values of $K_{g,atp}$ and $K_{d,atp}$ can be determined by varying the nutrient uptake rates and measuring the cellular growth and death rates. If appreciable cell death is not observed until ATP production is low then $K_{g,atp}$ and $K_{d,atp}$ are in the lower regime and accurate determination of their values is not necessary. Alternatively, if $K_{g,atp}$ and $K_{d,atp}$ are located in the upper regime, near the maximum ATP production rate, then more careful estimation will be necessary.

The local sensitivity analysis for the nominal parameter values showed that $K_{g,atp}$ had a significant effect on the number of quiescent cells and $K_{d,atp}$ had a significant effect on the number of dead cells (Table 2). Both of these results were due to the large relative differences between the numbers of cells in each population. Throughout the spheroid, the total number of living cells decreased when $K_{g,atp}$ was increased. However, the total number of proliferating cells was an order of magnitude larger than the number of quiescent and dead cells. Therefore, a small change in the proliferating cell penetration depth resulting from the $K_{g,atp}$ perturbation induced a large change in the number of quiescent cells compared to the number of proliferating cells. Similarly, $K_{d,atp}$ had a larger relative

effect on total number of dead cells compared to the number of live cells.

3.2.3. Parameters for live and dead cell volumes

Local sensitivity analysis showed that the live cell volume, V_L , significantly affected all of the cell population metrics (Table 2), implying that different cell types with different nominal volumes would have significantly different survival metrics. These results can be explained by recognizing that the live cell volume determines the characteristic length scale for the model. The increase in the live cell volume reduced the number of cells per unit volume, reduced the nutrient uptake per volume, and subsequently increased nutrient penetration. Therefore, increased V_L causes deeper penetration of both proliferating and quiescent cells into the spheroid. The dead cell volume fraction, δ , significantly affected the quiescent cell penetration depth and the total number of dead and quiescent cells (Table 2). Because this parameter represents the volume ratio of dead to live cells, the primary effect of perturbations was to change the location of the boundary between live and dead cells. Therefore, δ had a significant impact on the metrics associated with this boundary: the quiescent cell penetration depth and the dead and quiescent cell numbers. These results suggest that careful determination of live and dead cell volumes within 3-D cultures is necessary to accurately predict the quiescent cell population.

4. Conclusions

The tumor spheroid growth model described herein has incorporated many facets of tumor physiology that enable prediction of cell population distributions based solely on parameters describing individual cell characteristics. The cell population distribution is clinically important because it relates to therapeutic efficacy. Unique aspects of our model include: (1) incorporation of intracellular energy metabolism; (2) inclusion of the diffusion and cellular uptake of multiple nutrients, including glucose, oxygen and lactate; and (3) parameterization of the cellular growth and death in terms of ATP production. The diffusion of nutrients has long been recognized as an important feature of tumor growth dynamics. With the exception of Casciari et al. (1992), previous models have been based on the assumption of a single growth-limiting nutrient. We constructed the present model to test the hypothesis that cellular metabolism plays a critical role in tumor cell population dynamics. The inclusion of cellular metabolism and multiple nutrients enabled the prediction of several phenomena that are commonly observed in tumors and spheroids, including high glycolytic rates, the presence of hypoxia, and high concentrations of lactate (Walenta et al., 2002).

Based on local and large perturbation sensitivity analysis, we found that the cellular parameters that have the greatest effect on the location and number of quiescent

cells in spheroids is the maximum oxygen uptake rate, $Q_{Ox,max}$, the normalized maximum death rate, Γ , the basal survival rate, σ , the live cell volume, V_L , and the dead-to-live cell volume ratio, δ . The distribution of quiescent cells is critical for predicting the efficacy of chemotherapeutics, which are generally ineffective against slowly growing and arrested cells not progressing through mitosis. At the nominal parameter values, most of which have an experimental basis, we observed that oxygen availability had a greater impact on the distribution of quiescent cells, than either glucose or lactate availability. We determined that a 25% decrease in the maximum glucose uptake rate or a 100% increase in the maximum oxygen uptake rate would invert this phenomenon and the distribution of quiescent cells would become strongly dependent on glucose availability. The observed dependence on oxygen availability was attributed to the inclusion of lactate absorption into our model. The normalized maximum death rate, Γ , and the basal survival rate, σ , significantly affected both the location and number of quiescent cells by shifting the location of viable cells within the spheroid. The live cell volume, V_L , and the dead-to-live cell volume fraction, δ , both affected the population of quiescent cells by changing the characteristic length scale for nutrient transport. Based on these model results we suggest that accurate experimental determination of these five critical cellular parameters is necessary to predict the cell population distribution within spheroids and to predict the efficacy of administered chemotherapeutics on in vivo tumors.

References

- Acker, H., Carlsson, J., Holtermann, G., Nederman, T., Nylen, T., 1987. Influence of glucose and buffer capacity in the culture medium on growth and pH in spheroids of human thyroid carcinoma and human glioma origin. *Cancer Res.* 47, 3504–3508.
- Adam, J.A., Maggelakis, S.A., 1989. Mathematical models of tumor growth. IV. Effects of a necrotic core. *Math. Biosci.* 97, 121–136.
- Adam, J.A., Maggelakis, S.A., 1990. Diffusion regulated growth characteristics of a spherical prevascular carcinoma. *Bull. Math. Biol.* 52, 549–582.
- Araujo, R.P., McElwain, D.L., 2004. A history of the study of solid tumour growth: the contribution of mathematical modelling. *Bull. Math. Biol.* 66, 1039–1091.
- Bertuzzi, A., D'Onofrio, A., Fasano, A., Gandolfi, A., 2003. Regression and regrowth of tumour cords following single-dose anticancer treatment. *Bull. Math. Biol.* 65, 903–931.
- Brizel, D.M., Scully, S.P., Harrelson, J.M., Layfield, L.J., Bean, J.M., Prosnitz, L.R., Dewhirst, M.W., 1996. Tumor oxygenation predicts for the likelihood of distant metastases in human soft tissue sarcoma. *Cancer Res.* 56, 941–943.
- Brizel, D.M., Schroeder, T., Scher, R.L., Walenta, S., Clough, R.W., Dewhirst, M.W., Mueller-Klieser, W., 2001. Elevated tumor lactate concentrations predict for an increased risk of metastases in head-and-neck cancer. *Int. J. Radiat. Oncol. Biol. Phys.* 51, 349–353.
- Brown, P.N., Hindmarsh, A.C., Petzold, L.R., 1994. Using Krylov methods in the solution of large-scale differential-algebraic systems. *SIAM J. Sci. Comput.* 15, 1467–1488.
- Brown, P.N., Hindmarsh, A.C., Petzold, L.R., 1995. DASP, Santa Barbara, CA.
- Byrne, H.M., Chaplain, M.A., 1995. Growth of nonnecrotic tumors in the presence and absence of inhibitors. *Math. Biosci.* 130, 151–181.
- Casciari, J.J., Sotirchos, S.V., Sutherland, R.M., 1988. Glucose diffusivity in multicellular tumor spheroids. *Cancer Res.* 48 (14), 3905–3909.
- Casciari, J., 1989. The effects of diffusion and reaction of nutrients and metabolic waste products on the growth and microenvironment of multicellular tumor spheroids. Ph.D. Dissertation, University of Rochester, Rochester.
- Casciari, J.J., Sotirchos, S.V., Sutherland, R.M., 1992. Mathematical modelling of microenvironment and growth in EMT6/Ro multicellular tumour spheroids. *Cell Proliferat.* 25, 1–22.
- Chaplain, M.A., Britton, N.F., 1993. On the concentration profile of a growth inhibitory factor in multicell spheroids. *Math. Biosci.* 115, 233–243.
- Crank, J., 1984. *Free and Moving Boundary Problems*. Clarendon Press, New York.
- Finlayson, B.A., 1980. *Nonlinear Analysis in Chemical Engineering*. McGraw-Hill International Book Co., New York.
- Freyer, J.P., 1988. Role of necrosis in regulating the growth saturation of multicellular spheroids. *Cancer Res.* 48, 2432–2439.
- Freyer, J.P., Sutherland, R.M., 1986. Regulation of growth saturation and development of necrosis in EMT6/Ro multicellular spheroids by the glucose and oxygen supply. *Cancer Res.* 46, 3504–3512.
- Greenspan, H.P., 1976. On the growth and stability of cell cultures and solid tumors. *J. Theor. Biol.* 56, 229–242.
- Helmlinger, G., Sckell, A., Dellian, M., Forbes, N.S., Jain, R.K., 2002. Acid production in glycolysis-impaired tumors provides new insights into tumor metabolism. *Clin. Cancer Res.* 8, 1284–1291.
- Hietanen, P., Blomqvist, C., Wasenius, V.M., Niskanen, E., Franssila, K., Nordling, S., 1995. Do DNA ploidy and S-phase fraction in primary tumour predict the response to chemotherapy in metastatic breast cancer? *Br. J. Cancer* 71, 1029–1032.
- Jackson, T.L., Byrne, H.M., 2000. A mathematical model to study the effects of drug resistance and vasculature on the response of solid tumors to chemotherapy. *Math. Biosci.* 164, 17–38.
- Kunz-Schughart, L.A., 1999. Multicellular tumor spheroids: intermediates between monolayer culture and in vivo tumor. *Cell Biol. Int.* 23, 157–161.
- Landry, J., Freyer, J.P., Sutherland, R.M., 1982. A model for the growth of multicellular spheroids. *Cell Tissue Kinet.* 15, 585–594.
- Mueller-Klieser, W.F., Sutherland, R.M., 1984. Oxygen consumption and oxygen diffusion properties of multicellular spheroids from two different cell lines. *Adv. Exp. Med. Biol.* 180, 311–321.
- Newsholme, A.E., Leech, A.R., 1983. *Biochemistry for the Medical Sciences*. Wiley, Chichester.
- Pettet, G.J., Please, C.P., Tindall, M.J., McElwain, D.L., 2001. The migration of cells in multicell tumor spheroids. *Bull. Math. Biol.* 63, 231–257.
- Sherratt, J.A., Chaplain, M.A., 2001. A new mathematical model for avascular tumour growth. *J. Math. Biol.* 43, 291–312.
- Siu, W.Y., Arooz, T., Poon, R.Y., 1999. Differential responses of proliferating versus quiescent cells to adriamycin. *Exp. Cell Res.* 250, 131–141.
- Smallbone, K., Gavaghan, D.J., Gatenby, R.A., Maini, P.K., 2005. The role of acidity in solid tumour growth and invasion. *J. Theor. Biol.* 235, 476–484.
- Sutherland, R.M., 1988. Cell and environment interactions in tumor microregions: the multicell spheroid model. *Science* 240, 177–184.
- Vaupel, P., Thews, O., Hoekel, M., 2001. Treatment resistance of solid tumors: role of hypoxia and anemia. *Med. Oncol.* 18, 243–259.
- Walenta, S., Salameh, A., Lyng, H., Evensen, J.F., Mitze, M., Rofstad, E.K., Mueller-Klieser, W., 1997. Correlation of high lactate levels in head and neck tumors with incidence of metastasis. *Am. J. Pathol.* 150, 409–415.
- Walenta, S., Wetterling, M., Lehrke, M., Schwickert, G., Sundfor, K., Rofstad, E.K., Mueller-Klieser, W., 2000. High lactate levels

- predict likelihood of metastases, tumor recurrence, and restricted patient survival in human cervical cancers. *Cancer Res.* 60, 916–921.
- Walenta, S., Schroeder, T., Mueller-Klieser, W., 2002. Metabolic mapping with bioluminescence: basic and clinical relevance. *Biomol. Eng.* 18, 249–262.
- Warburg, O., 1929. Ist die aerobe Glykolyse spezifisch für die Tumoren. *Biochem. Z.* 204, 482–483.
- Ward, J.P., King, J.R., 1997. Mathematical modelling of avascular-tumour growth. *IMA J. Math. Appl. Med. Biol.* 14, 39–69.
- Ward, J.P., King, J.R., 1999. Mathematical modelling of avascular-tumour growth II. Modeling growth saturation. *IMA J. Math. Appl. Med. Biol.* 16, 171–211.
- Ward, J.P., King, J.R., 2003. Mathematical modelling of drug transport in tumour multicell spheroids and monolayer cultures. *Math. Biosci.* 181, 177–207.